Ain Shams Engineering Journal 17 (2026) 104382

Contents lists available at ScienceDirect

Ain Shams Engineering Journal

journal homepage: www.sciencedirect.com

Full Length Article

Levenberg–Marquardt neural network prediction of MHD hybrid nanofluid flow between parallel plates: Aerospace applications

Gunisetty Ramasekhar [a,1], Maddina Dinesh Kumar [c,1], A. Divya [b], Nehad Ali Shah [d,1], Se-Jin Yook [c,*]

[a] Department of Mathematics, Rajeev Gandhi Memorial College of Engineering and Technology (Autonomous), Nandyal 518501, Andhra Pradesh, India
[b] Department School of Technology, The Apollo University, Chittoor, Andhra Pradesh 517127, India
[c] School of Mechanical Engineering, Hanyang University, 222 Wangsimni-ro, Seongdong-gu, Seoul 04763, the Republic of Korea
[d] Department of Mechanical Engineering, Sejong University, Seoul 05006, the Republic of Korea

ARTICLE INFO

Keywords:
Porous medium
Parallel plates
Hybrid Nanofluid
Magnetohydrodynamics
Thermal radiation
Computational simulation

ABSTRACT

Thermal performance is an important and common issue for today's aeronautic technology and electrically powered devices. The following problems are commonly encountered due to increased heat generation or decreased surface area for cooling (limitation). One possible way to overcome this exciting challenge is to create a suitable cooling system architecture or to enhance the thermal transfer process. In this regard, hybrid nanofluids can help resolve these problems. In this work, the machine learning-based numerical analysis of MHD hybrid nanofluid flow through a rocket engine nozzle considering the effects of radiation, viscous dissipation and porous media is proposed. The hybrid nanofluid is produced by mixing basic fluid (kerosene oil) with the nanoparticles Ag-SiO2-TiO2 (Ag- silica- titanium dioxide), which have been chosen for their outstanding thermophysical properties. Similarity transformations are used to define and solve the non-linear equations of momentum and energy and to guarantee stability and accuracy over a range of parametric regimes in the MATLAB bvp4c scheme. Considering important factors like Reynolds number (Re) and their effect on temperature distribution, skin friction, Nusselt number and velocity, the radiation, magnetic interaction, Eckert number and porosity are studied. When the thermal radiation and Eckert number values are rising, the thickness of the thermal boundary layer. The Levenberg–Marquardt technique optimises an Artificial Neural Network (ANN) to improve prediction capabilities. The ANN shows excellent agreement with numerical data, with correlation coefficients close to unity. The framework that has been suggested emphasises the significance of using hybrid nanofluids and data-driven methodologies to enhance rocket cooling efficiency and guarantee thermal stability in aerospace propulsion systems.

1. Introduction

Rocket propulsion systems are highly developed and function according to momentum conservation. This system releases high-speed exhaust gases to generate thrust in the opposite direction. These machines are basically fluid-driven since their principal energy source is derived from propellants that are either liquid or gaseous and kept in tanks. Liquid hydrogen and other cryogenic fuels, oxidisers like liquid oxygen and storable propellants like hydrazine are examples of the fluids that fall under this category. According to the data available till 2023, the design and performance of a rocket are governed by complex aspects of fluid dynamics. These aspects begin with the pressurization and delivery of propellants, followed by mixing and combustion within the chamber, and then the expansion of hot gases through a convergent–divergent nozzle to achieve supersonic jet velocities. A fluid's thrust, specific impulse, and overall efficiency are all directly influenced by fluid dynamic processes like turbulence, compressible gas dynamics, and boundary layer effects [1]. Fluids have a function in rockets that goes beyond just propelling the rocket forward. To prevent vaporisation and tank pressure instability, cryogenic propellants need precise temperature control for optimal performance. According to Daigle et al. [2],

* Corresponding author.
E-mail addresses: gunisettyrama@gmail.com (G. Ramasekhar), dineshmaddina319@gmail.com (M. Dinesh Kumar), divyareddy31191@gmail.com (A. Divya), nehadali199@yahoo.com (N.A. Shah), ysjnuri@hanyang.ac.kr (S.-J. Yook).
[1] These authors contributed equally to this work and are co-first authors.

https://doi.org/10.1016/j.asej.2026.104382
Received 5 October 2025; Received in revised form 20 June 2026; Accepted 18 July 2026
Available online 5 August 2026
2090-4479/© 2026 The Author(s). Published by Elsevier B.V. on behalf of Faculty of Engineering, Ain Shams University. This is an open access article under the CC BY-NC-ND license (http://creativecommons.org/licenses/by-nc-nd/4.0/).

Nomenclature

Symbol.	Description. Units
u	Velocity component along the (x)-direction. $m\ s^{-1}$
v	Velocity component along the (y)-direction. $m\ s^{-1}$
x,r	Cartesian coordinates. m
T	Fluid temperature. K
T_w	Wall temperature. K
T_∞	Ambient temperature. K
B	Applied magnetic field strength. T
q_r	Radiative heat flux. $W\ m^{-2}$
p	Pressure. Pa
k^*	Permeability of porous medium. m^2
$f(\eta)$	Dimensionless stream function. –
$\theta(\eta)$	Dimensionless temperature. –
C_f	Skin-friction coefficient. –
Nu_x	Local Nusselt number. –
τ_w	Wall shear stress. Pa
ϕ_1	Volume fraction of Au nanoparticles. –
ϕ_2	Volume fraction of TiO_2 nanoparticles. –
ϕ_3	Volume fraction of SiO_2 nanoparticles. –
η	Similarity variable. –
θ	Dimensionless temperature. –
μ	Dynamic viscosity. $Pa{\cdot}s$
υ	Kinematic viscosity. $m^2\ s^{-1}$
ρ	Density. $kg\ m^{-3}$
σ	Electrical conductivity. $S\ m^{-1}$
σ^*	Stefan–Boltzmann constant. $W\ m^{-2}\ K^{-4}$
M	Magnetic parameter. –
K	Porosity (permeability) parameter. –
Pr	Prandtl number. –
Rd	Thermal radiation parameter. –
Ec	Eckert number. –
Re	Reynolds number. –
H_1	Density ratio. –
H_2	Viscosity ratio. –
H_3	Heat-capacity ratio. –
H_4	Thermal conductivity ratio. –
H_5	Electrical conductivity ratio. –
MHD	Magnetohydrodynamics. –
ANN	Artificial Neural Network. –
LM	Levenberg–Marquardt Algorithm. –
$BVP4c$	MATLAB Boundary Value Problem Solver. –
Au	Gold nanoparticle. –
TiO_2	Titanium dioxide nanoparticle. –
SiO_2	Silicon dioxide nanoparticle. –
f	Base fluid. –
np	Nanoparticle. –
hnf	Hybrid nanofluid. –
w	Wall. –
∞	Ambient condition. –
r	Radiation. –

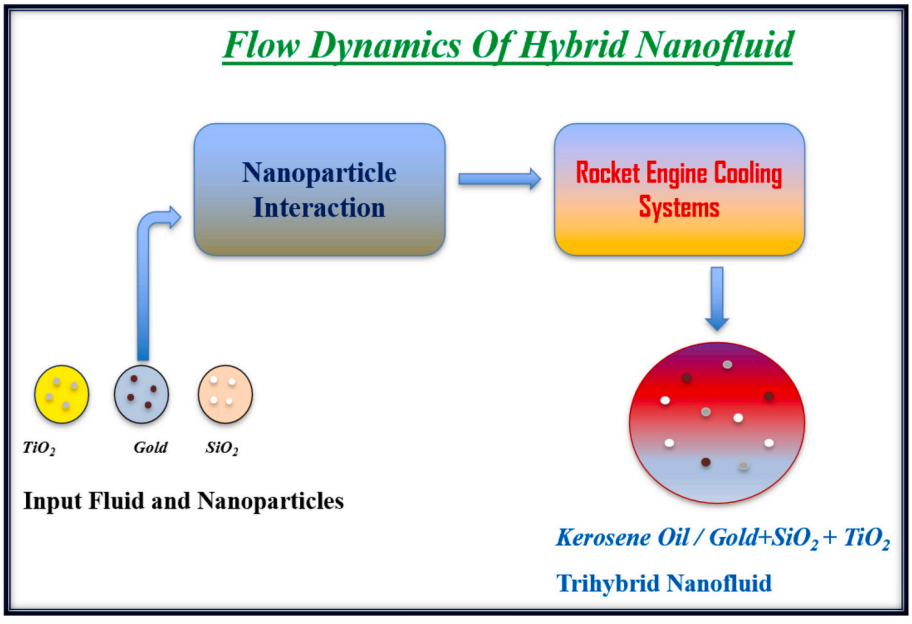


Fig. 1. Flow dynamics of hybrid nanofluid.

the need for accurate modelling of free-surface hydrodynamics arises because fluid sloshing inside large propellant tanks during manoeuvres might result in stability and control concerns. Also, regenerative cooling is often used to cool rocket engines, particularly high-performance liquid engines. This is a process which encompasses the recirculation of fuel around the combustion chamber and nozzle walls prior to injection. This enables the fluid to absorb the heat without damaging the rocket engine structure. In addition, multiphase flow processes, where fluid dynamics is closely coupled with thermodynamics and materials science topics, such as cavitation in turbo-pumps, shock-boundary layer interaction in nozzles and heat transfer, including radiative, conductive and convective heat transfer. The rockets can have different applications like space exploration, satellite placement, planetary missions, defence system etc. and they can make use of these fluid-mechanical principles. Rockets are an ideal object for the study of fluid dynamics under extreme conditions, as they are able to predict, control, and design fluid flow in propulsion systems. This capability continues to be an essential one in aerospace engineering. Two-dimensional nanofluid flow over a rocket

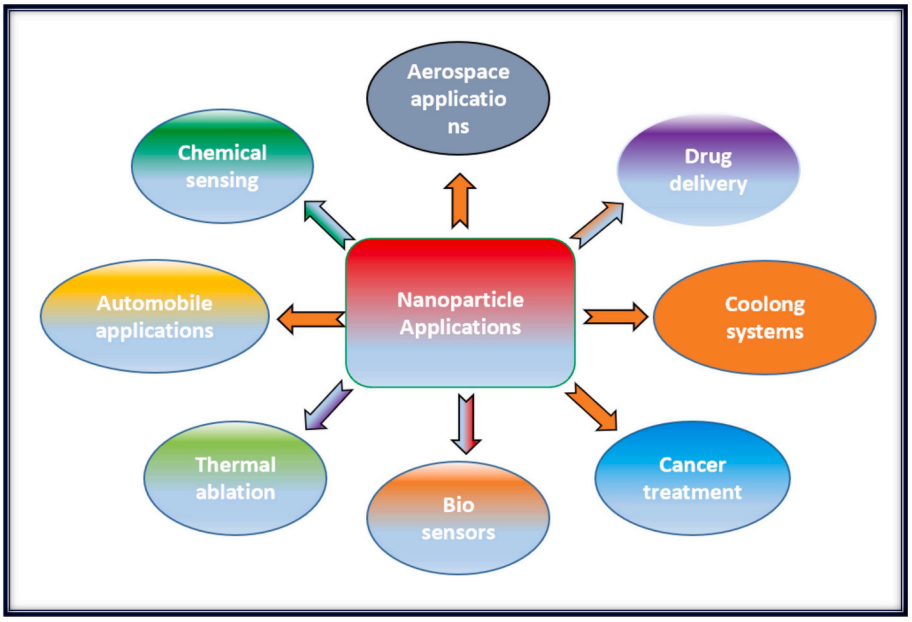


Fig. 2. Applications of hybrid nanofluid.

engine was the subject of a study conducted by Farood et al. [3]. The researchers strongly emphasised the evaluation of entropy production and the Bejan number to analyse thermodynamic irreversibility and heat transfer performance. Gasmi et al. [4] investigated improved cooling methods for rocket engines using hybrid nanofluids, considering melting heat transfer properties and second-order slip boundary effects. For aerospace cooling applications, Farooq et al. [5] studied the MHD flow of copper–ionic liquid nanofluid in Jeffery–Hamel geometry in order to investigate the improvement of heat transfer for a rocket nozzle, In the study, the two different nanoparticles are placed in a rocket engine nozzle which is shown in Fig. 1.The proposed model has potential applications in the aerospace cooling system and thermal management system as shown in Fig. 2. Muhammad et al. [6] used deep learning to study the flow of aggregative and non-aggregative nanofluids in a liquid rocket engine nozzle. Their research showed the power of deep learning in predicting the behavior of a nanofluid flow in aerospace propulsion with high accuracy. The mechanisms of heat transmission and entropy formation in the regenerative cooling channels of a rocket engine were investigated by Ullah et al. [7].

Materials referred to as porous media consist of a solid matrix with interconnecting pores or gaps that permit the passage of liquid or gaseous substances. Some structural features of porous media that significantly affect fluid flow and the transfer of mass and heat through the material include porosity, permeability, tortuosity, and pore size distribution [8]. Natural porous materials include soil, rocks, wood, and biological tissues; artificial porous materials include fibre networks, metal foams, packed beds, and porous ceramics. Porous media are often used in applications for better heat and mass transmission. For instance, heat exchangers and latent-heat thermal energy storage systems are included in heat exchangers to increase effective thermal conductivity and convective contact between fluid and solid phases. They are also essential to fuel cells, geothermal systems, drying technologies, soil evaporation, and hydrogen storage, all of which rely on the movement of mass and energy through porous materials [9]. In food engineering, prefabricated porous media are used in vacuum freeze-drying to expedite the drying process while maintaining the product's quality. This is accomplished by improving heat flow and moisture transfer [10]. To model transport phenomena in porous media, it may be necessary to apply Darcy's law (or extended non-Darcy models), take into account local thermal non-equilibrium (LTNE) between fluid and solid, incorporate radiative transfer, or resolve pore-scale effects versus macro scales. These requirements vary depending on the specific circumstances. The movement of nanofluids across porous media has been the research subject in recent times. Thermal performance may be further improved by introducing nanoparticles into the working fluid that saturates the pores; nevertheless, it is essential to consider the trade-offs that include higher viscosity, flow resistance, and increasing modelling complexity [11]. Divya and Anki Reddy [12] explored the behaviour of non-Newtonian fluid flow through a porous medium while exposed to the influence of a melting heat transport case.

A vital method of heat transport, thermal radiation occurs when matter's temperature causes energy to be released as electromagnetic waves. This process is critical at high temperatures. When temperature differentials are sizable or when materials or fluids exhibit substantial thermal radiation absorption, emission, or scattering, radiation may dominate or contribute alongside conduction and convection under various heat transport conditions. According to a recent study, heat flow and temperature fields may be significantly underestimated when thermal radiation is ignored in such settings. This is especially true when fluid media at solid–fluid interfaces absorb radiation. Furthermore, improvements in numerical models have enhanced the coupling of thermal radiation with other transport phenomena, including magnetic fields, fluid flow, heat generation/absorption, and non-linear fluid property variations. Better modelling of non-linear and spectral radiation and integrating radiation with other effects are two critical themes highlighted by these discoveries. Accurately including thermal radiation, whether linear or non-linear, is becoming increasingly essential for most engineering applications, including high-temperature combustion, nuclear reactors, solar collectors, and aerospace systems, to achieve dependable design and safety margins. Kumar et al. [13] Examine the effects of radiation on convective Nusselt numbers under different optical thicknesses and scattering albedos in a three-dimensional domain that contains both fluid and solid parts. Rashad et al. [14] Investigate the effects of radiation on natural convection in a porous, wavy cavity shape that incorporates hybrid nanofluids and magnetic fields. Majeed et al. [15] Investigate how nanofluids' electrical conductivity and radiative effects improve heat transport, particularly in intense radiation and temperature gradients. Qureshi et al. [16] investigated artificial neural network-based numerical modelling using a polymer/CNT hybrid nanofluid, taking into account activation energy and MHD effects over

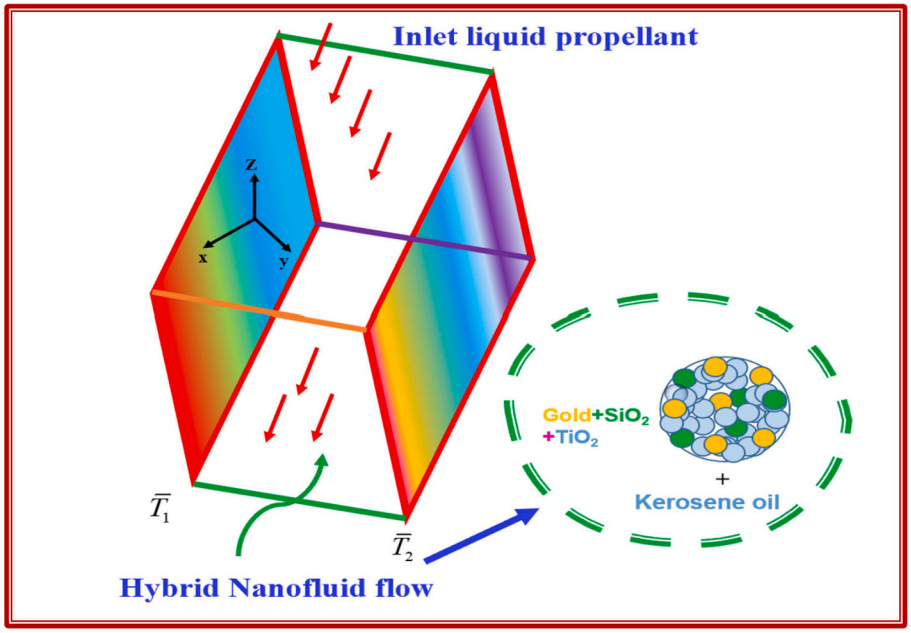


Fig. 3. Flow geometry of the model.

Table 1
Hybrid nanoparticles of thermo-physical properties Sakkaravarthi et al. [32], Singh et al. [33] and Mahanta et al.[34].

Property	Kerosene oil	Gold	TiO_2	SiO_2
$\rho(kgm^{-3})$	783	19,320	4250	2270
$C_p(Jkg^{-1}K^{-1})$	2090	129	686.2	730
$k_f(Wm^{-1}K^{-1})$	0.145	314	8.953	1.4013
$\sigma(sm^{-1})$	21×10^{-6}	4.10×10^{7}	2.6×10^{6}	3.5×10^{6}

Table 2
Comparison study of different values of Rd with (VIM method and ADM method) with present results (Bvp4c).

Rd	Previous study of Acharya et al.[37]	Previous study of Pattnaik et al. [35]	Present results (Bvp4c)
0	1.236554	1.23654563	1.23654501
1	1.119781	1.11974342	1.11974063
2	1.079337	1.07935434	1.07935104
3	1.067781	1.06774768	1.06774597

rotating surfaces. Using a stochastic machine learning approach, Zubair et al. [17] examine the heat and flow properties of a ternary-hybrid nanofluid that aggregates. In recent years, energy scarcity has become a major problem for industry since a large portion of the electricity produced is lost as heat during transmission. Wang et al. [18] in this study developed artificial neural network (ANN)-based prediction models for the thermal conductivity of hybrid nanofluids in waste heat systems. Parida et al. [19] studied the penta-hybrid nanofluid flow with entropy optimisation by using a multilayer neural network. They studied its use in improving heat transfer in the cooling of rocket engine nozzles. Khan et al. [20] used neural network to study the Soret–Dufour, bioconvection and double stratification effects on ternary hybrid nanofluid flow over a nonlinear radiative inclined cylinder. They looked at the resulting flow and heat transfer characteristics. Mahmood et al. [21] numerically and artificially intelligently studied the entropy generation of an inclined cylinder in the flow of MHD Jeffery tetra nanofluid. They studied its significance in the field of energy engineering applications and heat transfer. Wan et al. [22] developed a hybrid deep learning model for robust aeroengine remaining useful life prediction. They showed that it is a viable method for increasing the accuracy and reliability of predictions Liu et al. [23] gave an overview of deep learning surrogate models for aerodynamic optimization of airfoils and blade profiles. They identified their contribution to efficient aerodynamic design and prediction. Haq et al. [24] analyzed the Cross hybrid radiative and stratified bioconvective flow of a nanofluid in a porous medium of Darcy–Forchheimer type under Lorentz forces. They studied its effect on the fluid flow/heat transfer properties. Saleem et al. [25] explored the entropy generation in bioconvective micropolar hybrid nanofluid flow for activation energy and Lorentz force. These parameters were studied for their influence on the thermal and flow properties. Kong et al. [26] studied numerically the particle deposition and heat transfer in an S-shaped miniature cooling channel of a gas turbine blade. They studied its effect on cooling capacity and thermal properties. Le et al. [27] investigated the heat transfer in a mesh-fed slot cooling system using different height slots and different pin–fin configurations. They assessed the effects of these parameters on cooling performance. Rahman et al. [28] investigated the entropy generation analysis of magnetized mixed convection flow of Sutterby nanofluid containing chemical reaction. It was used to investigate its flow and heat transfer characteristics. Khouqeer et al. [29] studied the thermo-bioconvective ternary hybrid nanofluid flow over a rotating disk with activation energy. They studied its impacts on flow and thermal transport properties. The work by Ahmad et al. [30] investigated the localization of magnetic field and vortex formation of tetra-hybrid nanofluid flow by applying machine learning and numerical simulation. They looked at how they affect the flow and heat transfer properties. Zafar et al. [31] have studied the water-based tetra hybrid nanofluid flow over a shrinking cylinder with variable electrical conductivity and thermal radiation with the help of deep learning. They analysed the effects on flow and heat transfer characteristics.

Under high mechanical and thermal loads, rocket propulsion systems depend on efficient cooling and flow control to remain stable and functional. Traditional cooling methods often can't handle the combined effects of magnetic fields, radiation, viscous dissipation, and porous materials in rocket geometries. Because hybrid nanofluids have better

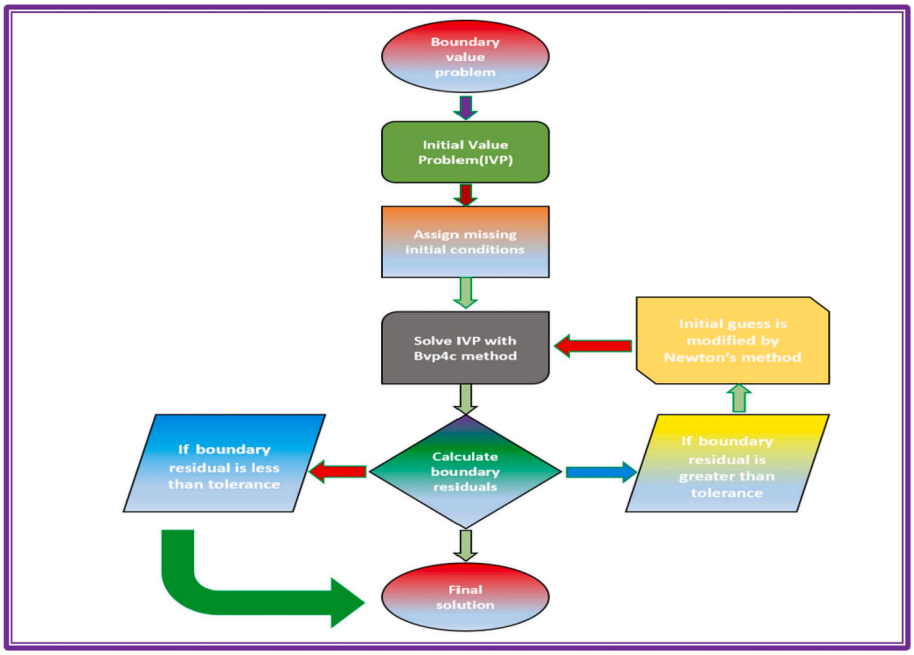


Fig. 4a. Numerical procedure.

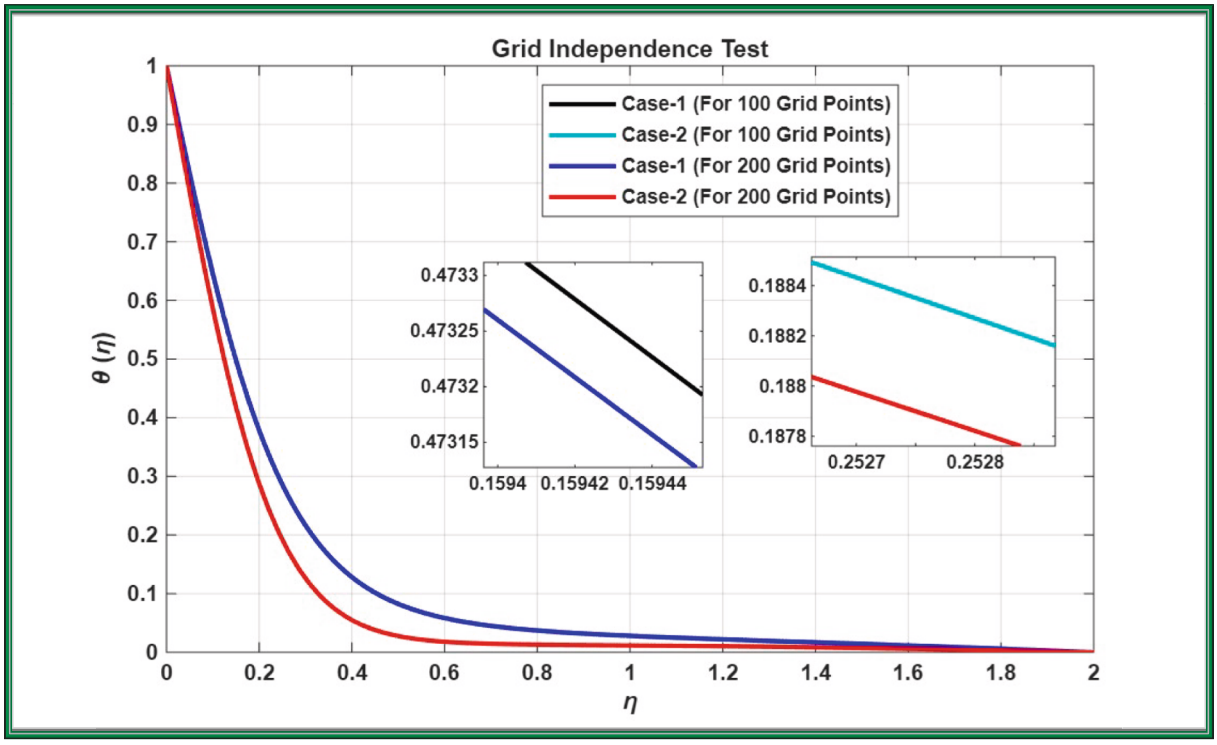


Fig. 4b. Grid Independence Test.

heat transmission and increased thermal conductivity, they have become attractive working fluids to solve these issues. The rapidly evolving computational methods, especially machine learning models and numerical solvers, offer reliable tools for the study of nonlinear flow behavior and improvements in thermal performance. The work is driven by the need for a comprehensive framework that integrates predictive modelling and better fluid characteristics to guarantee effective heat transfer, lower drag, and increased rocket engine performance.

1.1. Research questions

- How does the applied magnetic field impact the velocity transport and velocity distribution of the two cases hybrid nanofluid flow?
- What is the mixed influence of MHD, radiation, porosity, and viscous dissipation on heat-transfer performance?
- Can the proposed two cases hybrid nanofluids provide greater thermal-management performance for aerospace cooling uses?

- Can the Bvp4c computational framework precisely capture the highly nonlinear transport phenomena connected with the current model?
- Can the developed computational framework serve as a dependable tool for the design and optimization of innovative aerospace cooling structures?

1.2. Research objectives

- To develop a mathematical model for magnetohydrodynamic (MHD) hybrid nanofluid flow between parallel plates under the influence of thermal radiation, porous media, and viscous dissipation.
- To investigate the effects of magnetic parameter, Reynolds number, radiation parameter, porosity parameter, and Eckert number on the velocity and energy profiles.
- To examine the impacts of governing parameters on engineering quantities such as skin-friction coefficient and Nusselt number.
- To evaluate the heat-transfer improvement competence of Au–TiO_2–SiO_2 ternary hybrid nanoparticles distributed in kerosene oil.
- To validate the ANN forecasts against the mathematical Bvp4c solutions and assess forecast accuracy.

2. Mathematical modelling

- Considered the steady laminar hybrid nanofluid flow among two horizontal plates located at a distance $y = 0$ and $y = h$, which is presented in Fig. 3.
- Take into consideration the heat transfer between hybrid nanoparticles and a continuous flow in a two-dimensional arrangement. As a means of cooling the engine, the propellant is transported via a jacket that encircles the combustion area and the nozzle tip. Because the fuels or, on certain occasions, the oxidising agent could serve as great cooling fluids, which is an innovative idea.
- Viscous dissipation, thermal radiation, porous medium and MHD are considered.
- In the present article, Gold-Silicon dioxide-TiO2 Nanoparticles and base fluid, such as Kerosene oil, are considered, and the thermo-physical properties are shown in Table 1.

The governing flow equations are from the studies of Pattnaik et al. [35], Ullah et al. [36] and Acharya et al. [37].

$$\frac{\partial \overline{u}}{\partial x}+\frac{\partial \overline{v}}{\partial y}=0, \tag{1}$$

$$\overline{u}\frac{\partial \overline{u}}{\partial x}+\overline{v}\frac{\partial \overline{u}}{\partial y}=-\frac{1}{\rho_{HNF}}\frac{\partial p}{\partial x}+\frac{\mu_{HNF}}{\rho_{HNF}}\left(\frac{\partial^2 \overline{u}}{\partial x^2}+\frac{\partial^2 \overline{u}}{\partial y^2}\right)-\frac{\mu_{HNF}}{\rho_{HNF}}\frac{\overline{u}}{k^*}-\frac{\sigma_{HNF}}{\rho_{HNF}}\left(B^2\overline{u}\right), \tag{2}$$

$$\overline{u}\frac{\partial \overline{v}}{\partial x}+\overline{v}\frac{\partial \overline{v}}{\partial y}=-\frac{1}{\rho_{HNF}}\frac{\partial p}{\partial y}+\frac{\mu_{HNF}}{\rho_{HNF}}\left(\frac{\partial^2 \overline{v}}{\partial x^2}+\frac{\partial^2 \overline{v}}{\partial y^2}\right)-\frac{\mu_{HNF}}{\rho_{HNF}}\frac{\overline{v}}{k^*}-\frac{\sigma_{HNF}}{\rho_{HNF}}\left(B^2\overline{v}\right), \tag{3}$$

$$\overline{u}\frac{\partial \overline{T}}{\partial x}+\overline{v}\frac{\partial \overline{T}}{\partial y}=\frac{k_{HNF}}{(\rho c_p)_{HNF}}\left(\frac{\partial^2 \overline{T}}{\partial x^2}+\frac{\partial^2 \overline{T}}{\partial y^2}\right)+\frac{\mu_{HNF}}{(\rho c_p)_{HNF}}\left[2\left(\left[\frac{\partial \overline{u}}{\partial x}\right]^2+\left[\frac{\partial \overline{v}}{\partial y}\right]^2\right)+\left(\frac{\partial \overline{u}}{\partial y}+\frac{\partial \overline{v}}{\partial x}\right)^2\right]-\frac{1}{(\rho c_p)_{HNF}}\left(\frac{\partial q_r}{\partial y}\right). \tag{4}$$

By Rosseland approximation from Pattnaik et al. [35].

$$q_r=-\frac{4\sigma^*}{3k^*}\frac{\partial \overline{T}^4}{\partial y}. \tag{5}$$

Through the application of the Taylor series expansion for $\overline{T}^4$ and $\overline{T}_2$(and neglecting higher-order terms), we get

$$\overline{T}^4=4\overline{T}_2^3\overline{T}-3\overline{T}_2^4. \tag{6}$$

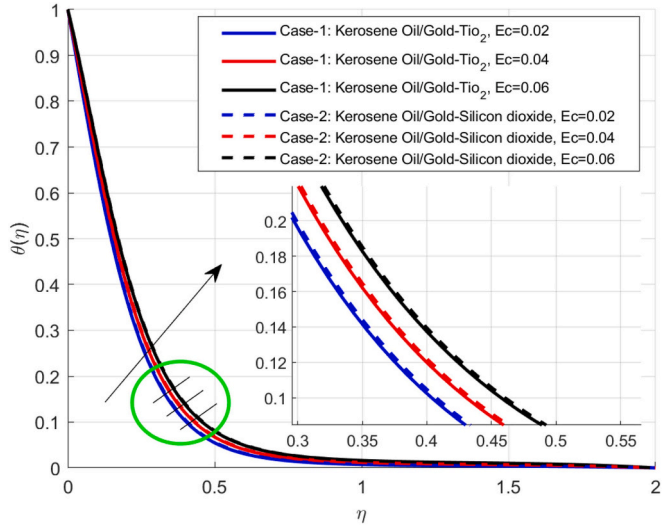


Fig. 5a. Repercussion of on

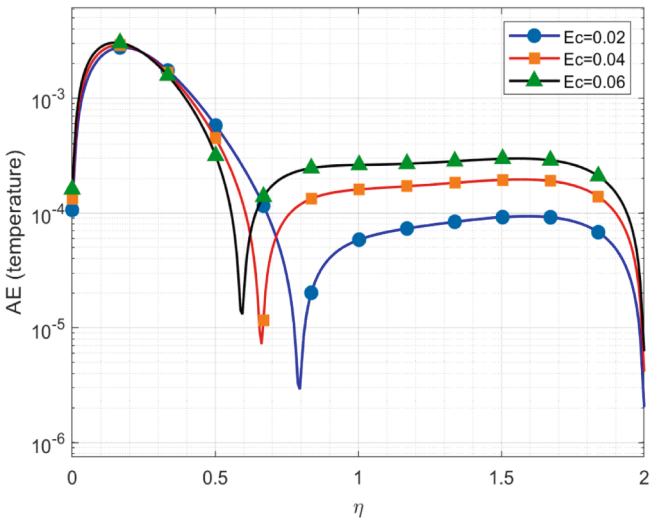


Fig. 5b. Absolute error of on

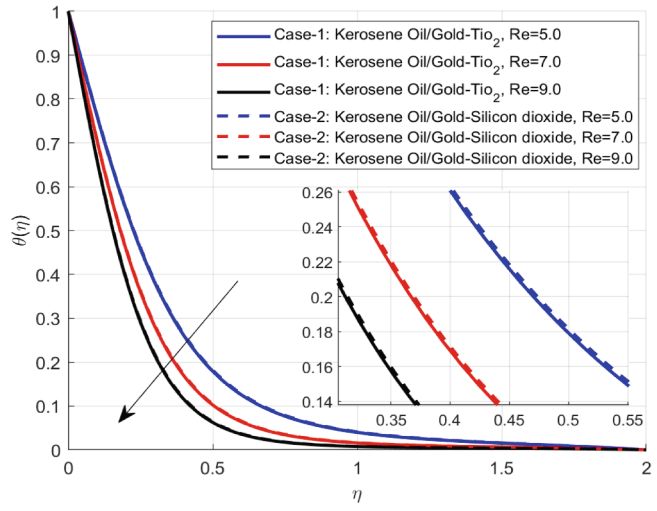


Fig. 6a. Repercussion of on

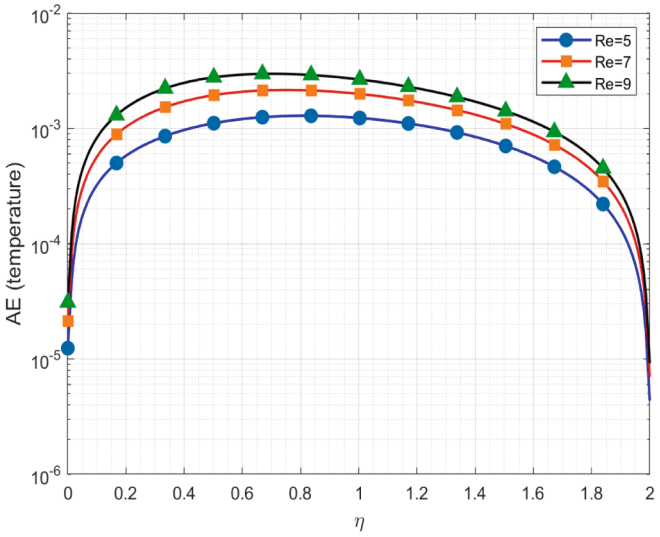


Fig. 6b. Absolute error of on

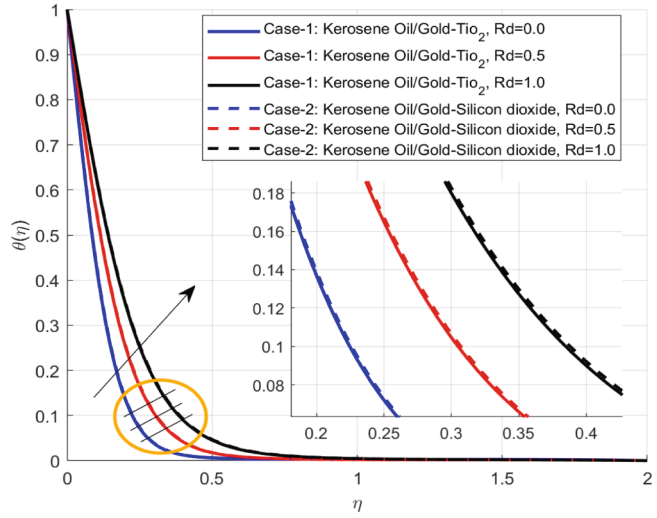


Fig. 7a. Repercussion of on

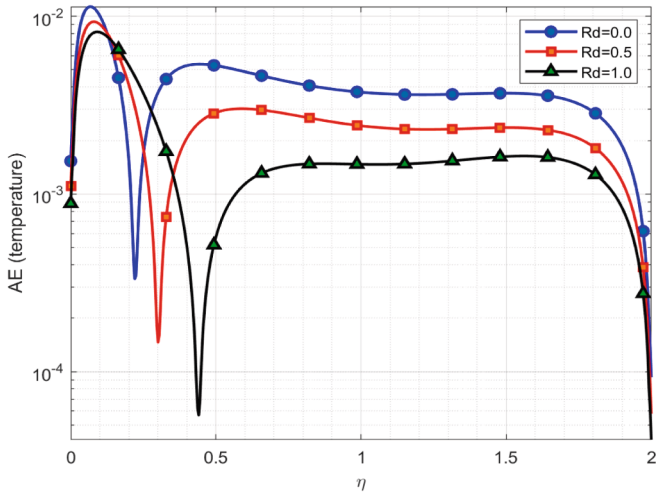


Fig. 7b. Absolute error of on

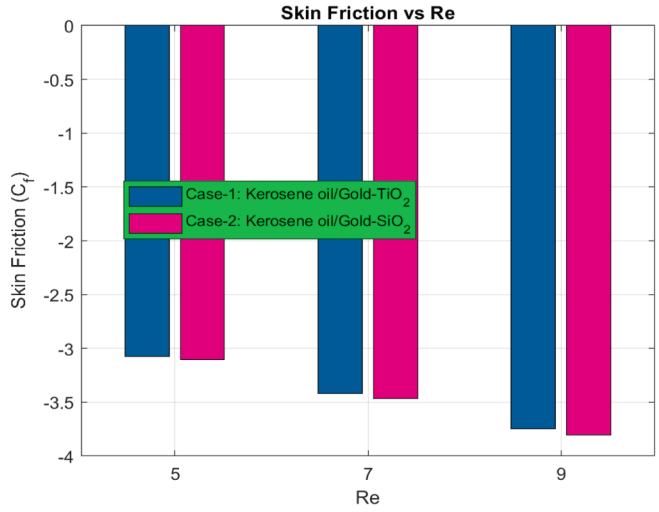


Fig. 8. Repercussion of on Cf.

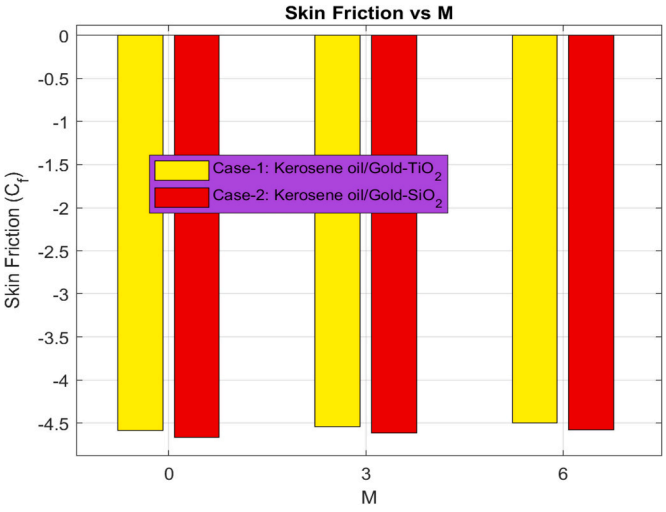


Fig. 9. Repercussion of on Cf.

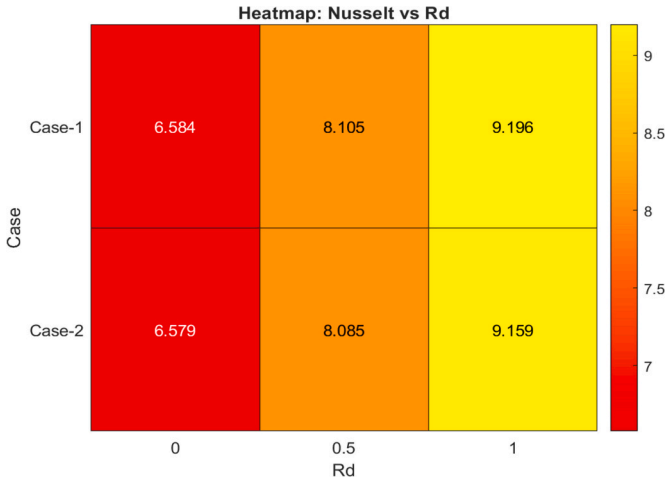


Fig. 10. Repercussion of Nusselt vs Rd.

By substituting Eqn. (5) and (6) in Eqn. (4), we get

$$\overline{u}\frac{\partial \overline{T}}{\partial x}+\overline{v}\frac{\partial \overline{T}}{\partial y}=\frac{k_{HNF}}{(\rho c_p)_{HNF}}\left(\frac{\partial^2 \overline{T}}{\partial x^2}+\frac{\partial^2 \overline{T}}{\partial y^2}\right)+\frac{\mu_{HNF}}{(\rho c_p)_{HNF}}\left[2\left(\left[\frac{\partial \overline{u}}{\partial x}\right]^2+\left[\frac{\partial \overline{v}}{\partial y}\right]^2\right)+\left(\frac{\partial \overline{u}}{\partial y}+\frac{\partial \overline{v}}{\partial x}\right)^2\right]+\frac{1}{(\rho c_p)_{HNF}}\frac{16\sigma^* T_2^3}{3k^*}\left(\frac{\partial^2 \overline{T}}{\partial y^2}\right). \tag{7}$$

The appropriate boundary constraints are

$$\begin{aligned}&\overline{u}=U=ax,\ \overline{v}=0,\ \overline{T}=\overline{T}_1, && at\ y=0\\ &\overline{u}=0,\ \overline{v}=0,\overline{T}=\overline{T}_2 && at\ y=h.\end{aligned} \tag{8}$$

The similarities are:

$$\begin{aligned}&\overline{u}=axf'(\eta),\overline{v}=-ahf(\eta),\\ &\theta(\eta)=\frac{\overline{T}-\overline{T}_2}{\overline{T}_1-\overline{T}_2},\eta=\frac{y}{h}.\end{aligned} \tag{9}$$

The thermophysical attributes of HNF include:

$$H_1=\frac{\rho_{HNF}}{\rho_f},H_2=\frac{\mu_{HNF}}{\mu_f},\ H_3=\frac{(\rho c_p)_{HNF}}{(\rho c_p)_f},H_4=\frac{k_{HNF}}{k_f},H_5=\frac{\sigma_{HNF}}{\sigma_f}. \tag{10}$$

The transformed dimensionless equations are

$$f^{iv}-\mathrm{Re}\frac{H_1}{H_2}[(f')f''-f'''\,]-\frac{H_1}{H_2}Kf''-\frac{H_5}{H_2}M(f'')=0, \tag{11}$$

$$\theta''\left(1+\frac{4}{3}\frac{Rd}{H_4}\right)+\frac{H_2}{H_1}\frac{H_3}{H_4}Pr\left(\mathrm{Re}\frac{H_1}{H_2}f\theta'+4Ec\frac{H_1}{H_3}[f']^2\right)=0. \tag{12}$$

The boundary conditions now take the form

$$\begin{aligned}&f=0,f'=1,\theta=1\ \ at\ \eta=0,\\ &f=0,f'=0,\theta=0\ \ at\ \eta=1.\end{aligned} \tag{13}$$

Note:$M=\frac{\sigma_f B^2}{\rho_f a}$, $Pr=\frac{\mu_f(\rho c_p)_f}{k_f\rho_f}$, $K=\frac{\upsilon}{k^* a}$,$Rd=\frac{4\sigma^*\overline{T}_2}{k^* k_f}$,$\mathrm{Re}=\frac{ah^2}{\upsilon_f}$,$Ec=\frac{\rho_f(ah)^2}{(\rho c_p)_f(\overline{T}_2-\overline{T}_1)}$ are Magnetic parameter, Prandtl number, Porosity parameter, Radiation parameter, Viscosity parameter, and Eckert number.

The dimensional form of C_f, and Nu are defined as

$$C_f=\frac{\tau_w}{\rho_f U^2} \tag{14}$$

where shear stress τ_w is $\tau_w=\mu_{HNF}\frac{\partial \overline{u}}{\partial y}\Big|_{y=0}$,

$$Nu=\frac{-hk_{HNF}\left(\frac{\partial \overline{T}}{\partial y}\right)_{y=0}-q_r}{k_f(\overline{T}_2-\overline{T}_1)}. \tag{15}$$

The dimensionless skin friction coefficient and Nusselt number are

$$Cf=H_2 f''(0), \tag{16}$$

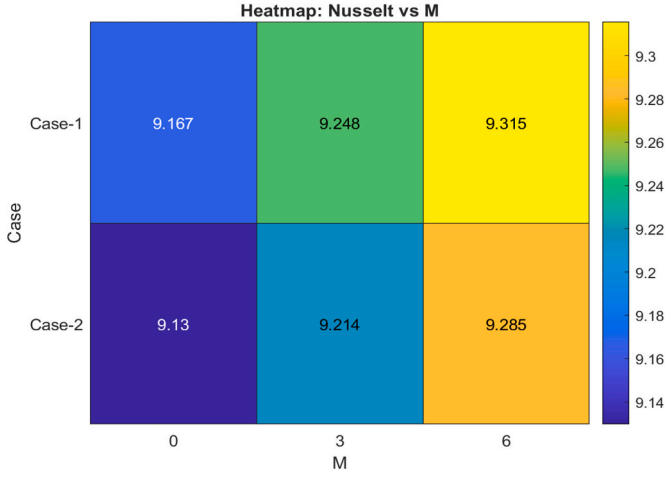


Fig. 11. Repercussion of Nusselt vs M.

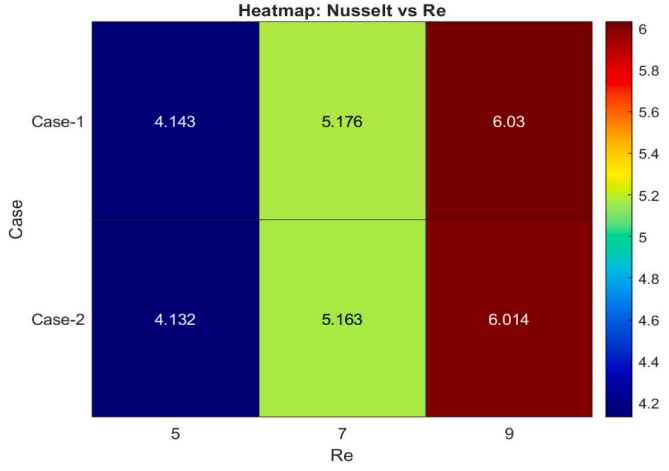
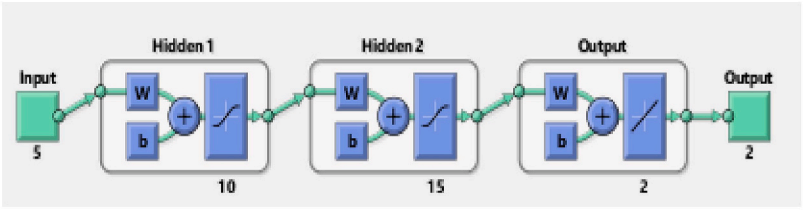


Fig. 12. Repercussion of Nusselt vs Re.



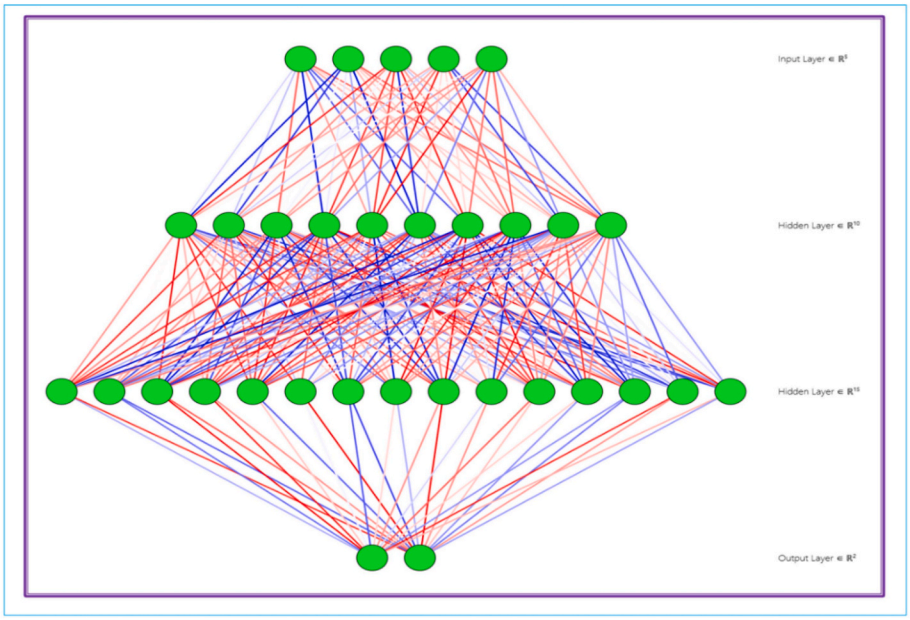


Fig. 13. ANN arcitchure.

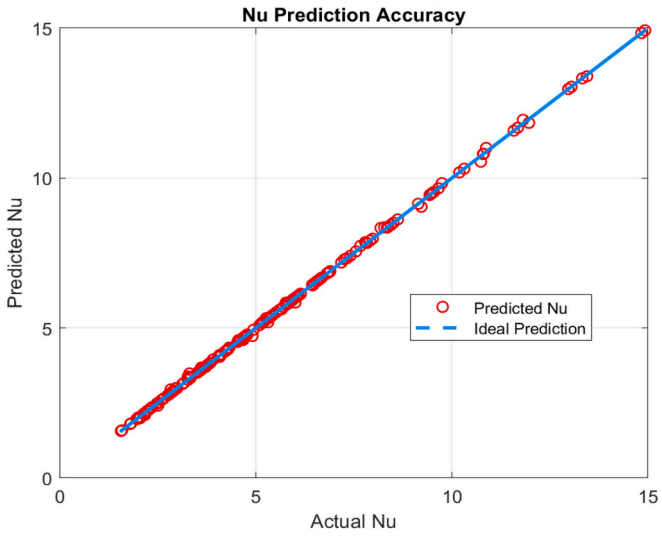


Fig. 14. Representation for Nu prediction accuracy.

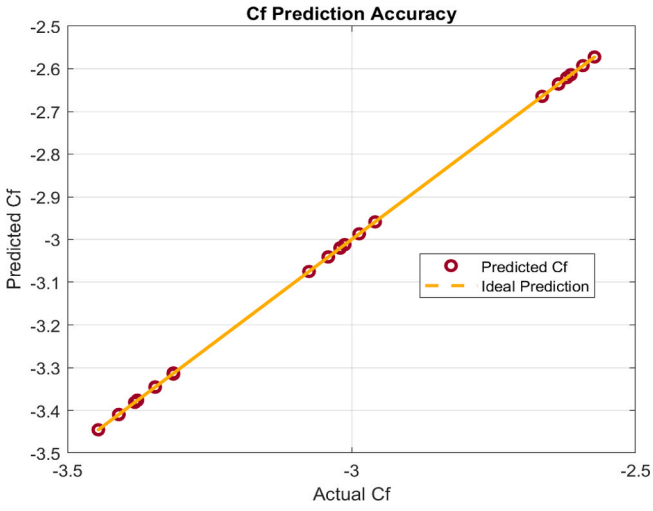


Fig. 15. Representation for Cf prediction accuracy.

$$Nu = -\left[H_4 + \frac{4}{3}Rd\right]\theta'(0). \tag{17}$$

3. Numerical procedure

The set of highly nonlinear ordinary differential equations (11)–(12), along with BCs (13), they are projected in MATLAB software with the help of the bvp4c method. To provide mesh-free confirmation, the integration of divided outcomes is required. For $\eta_{\max} = 2$, asymptotic convergence is observed in all graphs. The bvp4c method is a BVP solution involved in the MATLAB tool. The computational estimates of the momentum and energy profiles are derived with an accuracy tolerance of $\mathbf{10^{-6}}$. Comparison results are presented in Table 2, and the numerical procedure is shown in Fig. 4(a).

For computations, we used the appropriate assumptions as follows.

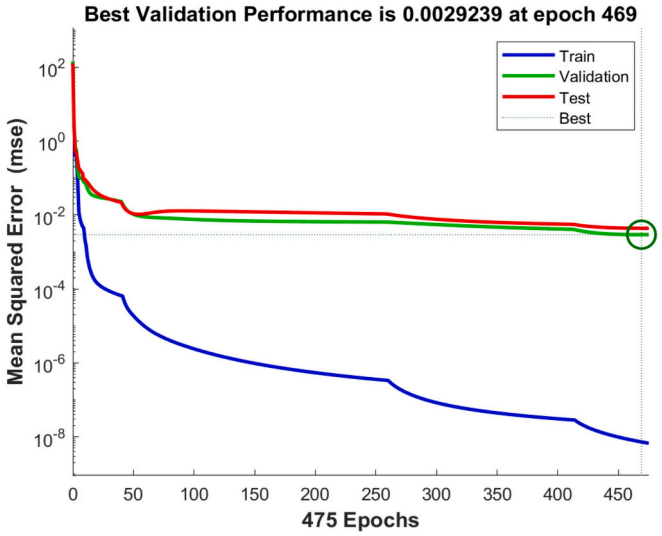


Fig. 16. Representation for Best validation

$$f^{iv} = -\left(-\mathrm{Re}\frac{H_1}{H_2}[(f')f'' - ff'''] - \frac{H_1}{H_2}Kf'' - \frac{H_5}{H_2}M(f'')\right),$$

$$\theta'' = -\left(\frac{\frac{H_2}{H_1}\frac{H_3}{H_4}Pr\left(\mathrm{Re}\frac{H_1}{H_2}f\theta' + 4Ec\frac{H_1}{H_3}[f']^2\right)}{\left(1+\frac{4}{3}\frac{Rd}{H_4}\right)}\right),$$

$$f = 0, f' = 1, \theta = 1 \quad at\ \eta = 0,$$

$$f = 0, f' = 0, \theta = 0 \quad at\ \eta = 1.$$

Let us consider

$$\left.\begin{array}{c} f = y_1, f' = y_2, f'' = y_3 \\ f''' = y_4, f^{iv} = y_4', \\ \theta = y_5, \theta' = y_6, \theta'' = y_6' \end{array}\right\},$$

$$y_4' = -\left(\mathrm{Re}\frac{H_1}{H_2}[(y_2)y_3 - y_1y_4] - \frac{H_1}{H_2}Ky_3 - \frac{H_5}{H_2}My_3\right),$$

$$y_6' = -\left(\frac{\frac{H_2}{H_1}\frac{H_3}{H_4}Pr\left(\mathrm{Re}\frac{H_1}{H_2}y_1y_6 + 4Ec\frac{H_1}{H_3}[y_2]^2\right)}{\left(1+\frac{4}{3}\frac{Rd}{H_4}\right)}\right),$$

$$y_1 = 0, y_2 = 1, y_5 = 1 \quad at\ \eta = 0,$$

$$y_1 = 0, y_2 = 0, y_5 = 0 \quad at\ \eta = 1.$$

Grid Independence Test: The temperature profile is shown in Fig. 4(b) for both 100 and 200 grid points, which shows good agreement between the two, thus demonstrating that the solutions are grid independent, accurate and numerically stable.

4. Results and Discussion

4.1. Numerous Elements Affecting the Temperature, velocity Profiles, error Analysis, and heat map plots

The current study investigated non-linear flow dynamics across a rocket geometry by considering the impacts of magnet m, radiation, viscous dissipation, porous effect, and modified governing equations using BVP4C in MATLAB software. Tables and graphs are used to illustrate the findings. Fig. 5(a) gives the influence of the Eckert number Ec on the temperature profile. It is noted that, as the Ec is higher, the temperature profile rises due to higher viscous dissipation and heating of the body. The trend is essential in the rocket geometry systems where high-velocity flows are known to considerably increase the boundary layer's thermal effects. Fig. 5(b) shows that the Eckert number Ec impacts the absolute error of the temperature profile. As can be seen, the Ec has a direct proportional relationship with the absolute error, i.e. the viscous dissipation has more substantial thermal effects. This confirms the strength of the numerical method in the rocket geometry problems in

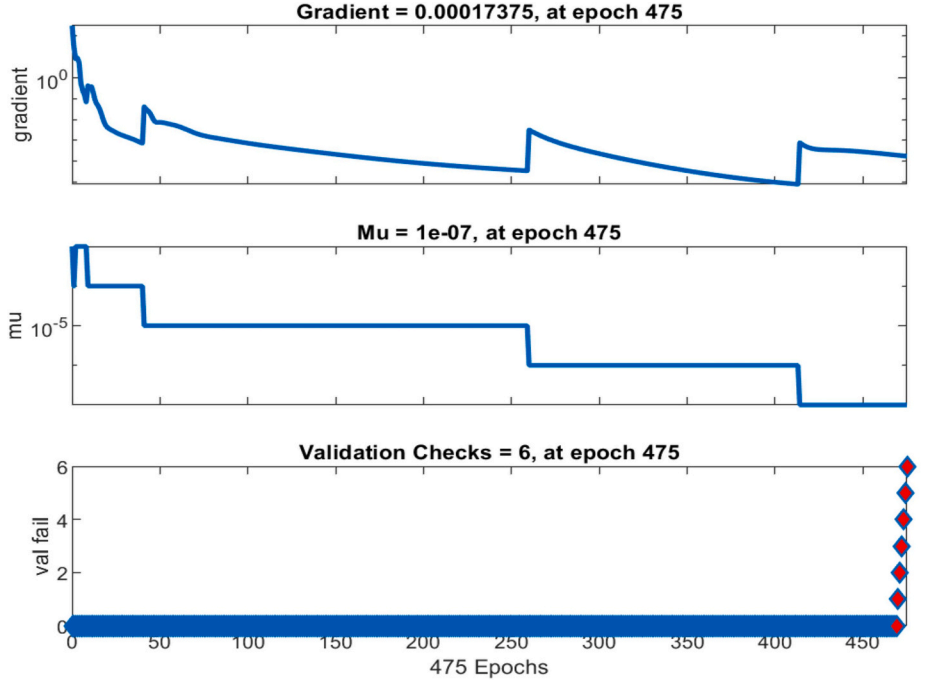


Fig. 17. Representation for gradient, mu, val fail.

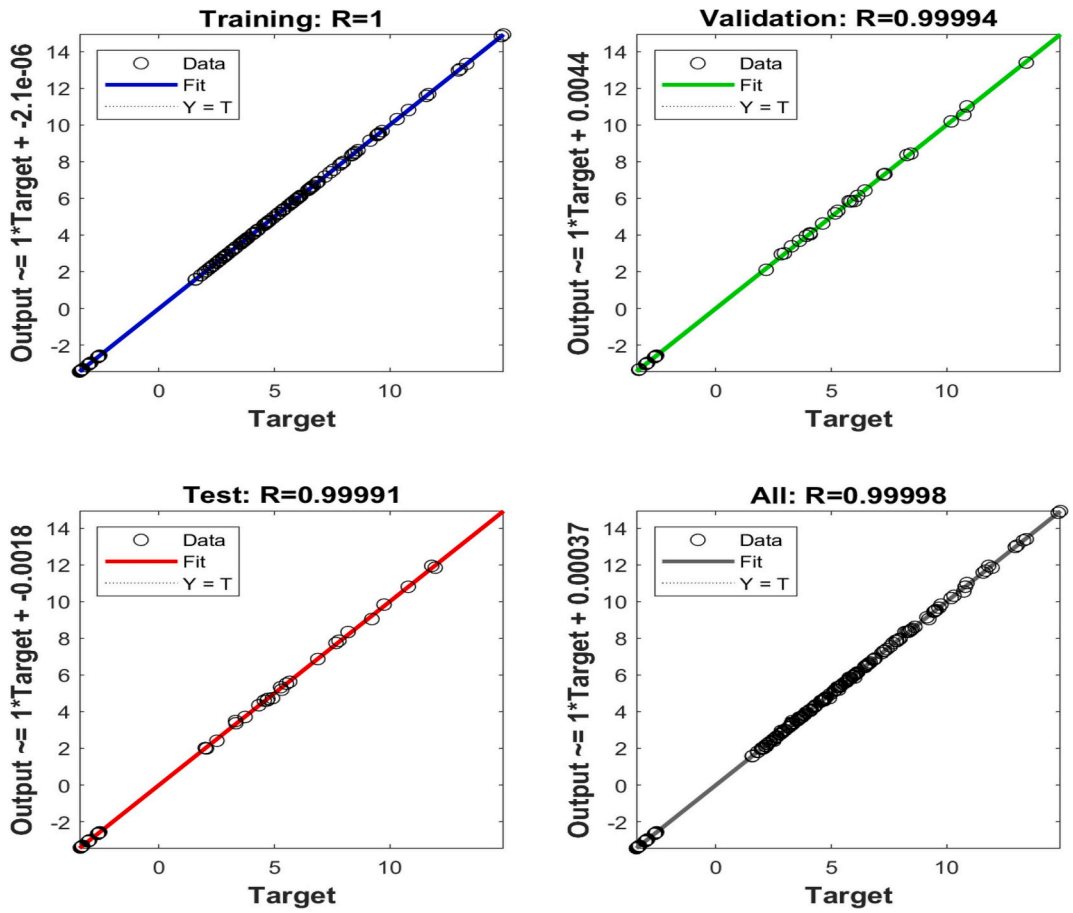


Fig. 18. Representation for over all performance model.

which the high flow speeds generate significant heating. The temperature profile at various Reynolds numbers Re is given in Fig. 6(a)**.** It is noted that with increased Re, the temperature profile reduces, meaning that the thermal boundary layer thickness decreases. Exploring geometry applications in which increased Reynolds numbers can boost convectional heat transfer and cooling is essential. Fig. 6(b) shows that the Reynolds number Re affects the absolute error of the temperature profile. It is observed that the absolute error grows, and the variations in the heat transfer predictions are more substantial. This proves the validity and consistency of the numerical model in rocket geometry, in the higher regimes of flow. Fig. 7(a) indicates the temperature profile as a function of the radiation parameter Rd. It is noted that the higher the Rd is, the higher the temperature profile, meaning that there is an increase in thermal energy transport. This is a very relevant trend in the application of rocket geometry, where radiation effects are significant in overall heat transfer the impact of the radiation parameter in Fig. 7(b)**.** Rd on the absolute error of the temperature profile is plotted.It is noted that as one increase, it becomes more. Rd, the relative error reduces, proving better numerical accuracy. This shows the computational stability of the method to calculate the rocket geometry whenever radiative heat transfer plays an important role. The results of Reynolds number Re on the skin friction are presented in Fig. 8.It is noted that the skin friction reduces steadily with increased Re. Additionally, the skin friction in Case-2 is relatively higher than in Case-1; this is crucial for rocket geometry design to ensure that the minimum drag is realised and that aerodynamic performance is enhanced. The influence of magnetic parameter M on the skin friction is displayed in Fig. 9**.** As the amount of M increases, the skin friction decreases. There is also more discrepancy in values between Case-2 and Case-1, which matters in the case of rocket geometry applications, where surface drag needs to be controlled. Fig. 10**,** the change of the Nusselt number with the radiation parameter. Rd is depicted. It is noted that with the increase of Rd, the Nusselt number also increases, demonstrating improved heat transfer. Moreover, the values are a bit higher in Case-1 than in Case-2, which is essential to the rocket geometry application, whereby an efficient thermal management must be undertaken. The influence of the

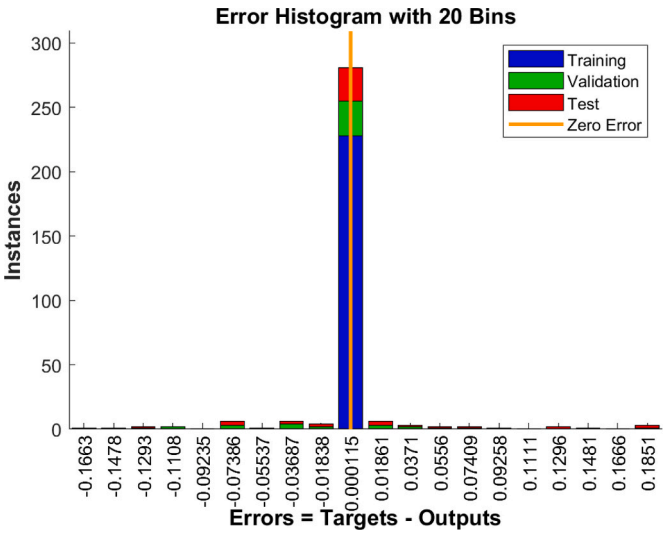


Fig. 19. Representation for Error Histogram.

Table 3
Table values for Skin friction actual vs ANN prediction.

M	Re	Ec	Rd	CaseID	Cf_actual	Cf_pred
1	5	0.02	1	1	−2.620894373	−2.620771686
1	5	0.02	2	1	−2.592736518	−2.592786917
1	5	0.02	3	1	−2.572303879	−2.572624468
1	5	0.04	1	1	−2.620894373	−2.620938381
1	5	0.04	2	1	−2.592736518	−2.592538688
1	5	0.04	3	1	−2.572303878	−2.572447194
1	5	0.06	1	1	−2.620894373	−2.620971142
1	5	0.06	2	1	−2.592736526	−2.592546807
1	5	0.06	3	1	−2.572303878	−2.572405813
1	7	0.02	1	1	−3.019953213	−3.019102311
1	7	0.02	2	1	−2.986639153	−2.986758989
1	7	0.02	3	1	−2.95850889	−2.958480438
1	7	0.04	1	1	−3.019953213	−3.019358406
1	7	0.04	2	1	−2.986639153	−2.986664969
1	7	0.04	3	1	−2.958508889	−2.958405341
1	7	0.06	1	1	−3.019953214	−3.019767488
1	7	0.06	2	1	−2.986639153	−2.986579845
1	7	0.06	3	1	−2.958508889	−2.958351717
1	9	0.02	1	1	−3.381514138	−3.381582575
1	9	0.02	2	1	−3.345756157	−3.345127158
1	9	0.02	3	1	−3.31362609	−3.313613043
1	9	0.04	1	1	−3.381514138	−3.381352107
1	9	0.04	2	1	−3.345756157	−3.345602299
1	9	0.04	3	1	−3.31362609	−3.314498671
1	9	0.06	1	1	−3.381514138	−3.381547295
1	9	0.06	2	1	−3.345756157	−3.345795792
1	9	0.06	3	1	−3.31362609	−3.315591017
3	5	0.02	1	1	−2.620894376	−2.621078825
3	5	0.02	2	1	−2.592736528	−2.592496091
3	5	0.02	3	1	−2.572303898	−2.5722249
3	5	0.04	1	1	−2.620894376	−2.620910371
3	5	0.04	2	1	−2.592736528	−2.59264722
3	5	0.04	3	1	−2.572303898	−2.572250038
3	5	0.06	1	1	−2.620894376	−2.621075976
3	5	0.06	2	1	−2.592736528	−2.592912465
3	5	0.06	3	1	−2.572303898	−2.5723295
3	7	0.02	1	1	−3.019953213	−3.019707265
3	7	0.02	2	1	−2.986639153	−2.986618585
3	7	0.02	3	1	−2.958508905	−2.958761372
3	7	0.04	1	1	−3.019953213	−3.019970813
3	7	0.04	2	1	−2.986639153	−2.986744607
3	7	0.04	3	1	−2.958508906	−2.958706103
3	7	0.06	1	1	−3.019953213	−3.020236468
3	7	0.06	2	1	−2.986639152	−2.98678062
3	7	0.06	3	1	−2.958508906	−2.958541273
3	9	0.02	1	1	−3.381514604	−3.381548227
3	9	0.02	2	1	−3.345756614	−3.345725355
3	9	0.02	3	1	−3.313626516	−3.312444567
3	9	0.04	1	1	−3.381514601	−3.381745794
3	9	0.04	2	1	−3.345756613	−3.345696074
3	9	0.04	3	1	−3.313626517	−3.313631851
3	9	0.06	1	1	−3.381514604	−3.381834148
3	9	0.06	2	1	−3.345756615	−3.345926051
3	9	0.06	3	1	−3.313626517	−3.314878454
5	5	0.02	1	1	−2.620892428	−2.62060181
5	5	0.02	2	1	−2.592733452	−2.592813796
5	5	0.02	3	1	−2.572300062	−2.572260871
5	5	0.04	1	1	−2.620892428	−2.620750665
5	5	0.04	2	1	−2.592733452	−2.5927183
5	5	0.04	3	1	−2.572300062	−2.572268744
5	5	0.06	1	1	−2.620892428	−2.620841734
5	5	0.06	2	1	−2.592733452	−2.592800973
5	5	0.06	3	1	−2.572300062	−2.572324283
5	7	0.02	1	1	−3.019952544	−3.019425272
5	7	0.02	2	1	−2.986638575	−2.986715828
5	7	0.02	3	1	−2.958508737	−2.958956643
5	7	0.04	1	1	−3.019952752	−3.02008863
5	7	0.04	2	1	−2.986638575	−2.986478475
5	7	0.04	3	1	−2.958508737	−2.958836497
5	7	0.06	1	1	−3.019952752	−3.020554055
5	7	0.06	2	1	−2.986637519	−2.986504057
5	7	0.06	3	1	−2.958508737	−2.958590268
5	9	0.02	1	1	−3.381514604	−3.381575529
5	9	0.02	2	1	−3.345756615	−3.345770533
5	9	0.02	3	1	−3.313626516	−3.313567798
5	9	0.04	1	1	−3.381514604	−3.381448194
5	9	0.04	2	1	−3.345756615	−3.346016673
5	9	0.04	3	1	−3.313626516	−3.313590389
5	9	0.06	1	1	−3.381514604	−3.381459517
5	9	0.06	2	1	−3.345756615	−3.346222042
5	9	0.06	3	1	−3.313626516	−3.3135988
1	5	0.02	1	2	−2.664489565	−2.664467343
1	5	0.02	2	2	−2.635593668	−2.635901597
1	5	0.02	3	2	−2.614095567	−2.61399986
1	5	0.04	1	2	−2.664489565	−2.664518405
1	5	0.04	2	2	−2.635593668	−2.635733609
1	5	0.04	3	2	−2.614095567	−2.614038829
1	5	0.06	1	2	−2.664489565	−2.6647865
1	5	0.06	2	2	−2.635593668	−2.635260896
1	5	0.06	3	2	−2.614095567	−2.613602294
1	7	0.02	1	2	−3.074828969	−3.074768868
1	7	0.02	2	2	−3.041036924	−3.041066386
1	7	0.02	3	2	−3.012152372	−3.01223615
1	7	0.04	1	2	−3.074828969	−3.074759826
1	7	0.04	2	2	−3.041036924	−3.041038981
1	7	0.04	3	2	−3.012152372	−3.012149945
1	7	0.06	1	2	−3.07482897	−3.074945357
1	7	0.06	2	2	−3.041036925	−3.041076409
1	7	0.06	3	2	−3.012152372	−3.011642195
1	9	0.02	1	2	−3.445797027	−3.446016734
1	9	0.02	2	2	−3.409749682	−3.409715747
1	9	0.02	3	2	−3.377111939	−3.377238966
1	9	0.04	1	2	−3.445797028	−3.445794807
1	9	0.04	2	2	−3.409749682	−3.409816074
1	9	0.04	3	2	−3.377111939	−3.376878339
1	9	0.06	1	2	−3.445797027	−3.44552316
1	9	0.06	2	2	−3.409749682	−3.409867874
1	9	0.06	3	2	−3.377111939	−3.376076863
3	5	0.02	1	2	−2.664489579	−2.664709444
3	5	0.02	2	2	−2.635593703	−2.635915629
3	5	0.02	3	2	−2.614095617	−2.614068328
3	5	0.04	1	2	−2.664489579	−2.664501675
3	5	0.04	2	2	−2.635593703	−2.635791755
3	5	0.04	3	2	−2.614095617	−2.614091489
3	5	0.06	1	2	−2.664489579	−2.664357684
3	5	0.06	2	2	−2.635593703	−2.635374828
3	5	0.06	3	2	−2.614095617	−2.61384857
3	7	0.02	1	2	−3.074828969	−3.074758368
3	7	0.02	2	2	−3.041036948	−3.041303181
3	7	0.02	3	2	−3.012152373	−3.012102997
3	7	0.04	1	2	−3.074828969	−3.074851938
3	7	0.04	2	2	−3.041036948	−3.041029517
3	7	0.04	3	2	−3.012152373	−3.012297599
3	7	0.06	1	2	−3.074828969	−3.074990254
3	7	0.06	2	2	−3.041036927	−3.041024089
3	7	0.06	3	2	−3.012152373	−3.012166464
3	9	0.02	1	2	−3.445797482	−3.445589507
3	9	0.02	2	2	−3.409750082	−3.409621788
3	9	0.02	3	2	−3.377112274	−3.376887963
3	9	0.04	1	2	−3.445797482	−3.445864068
3	9	0.04	2	2	−3.409750082	−3.40960179
3	9	0.04	3	2	−3.377112274	−3.377252713
3	9	0.06	1	2	−3.445797482	−3.445935037
3	9	0.06	2	2	−3.409750082	−3.409770464
3	9	0.06	3	2	−3.377112274	−3.377265499
5	5	0.02	1	2	−2.664484068	−2.664333455
5	5	0.02	2	2	−2.635593664	−2.636332332
5	5	0.02	3	2	−2.61409556	−2.61398735
5	5	0.04	1	2	−2.664484068	−2.664642118
5	5	0.04	2	2	−2.635593664	−2.636071998
5	5	0.04	3	2	−2.61409556	−2.614146966
5	5	0.06	1	2	−2.664484068	−2.664403816
5	5	0.06	2	2	−2.635585767	−2.635760019
5	5	0.06	3	2	−2.61409556	−2.614180718
5	7	0.02	1	2	−3.074827609	−3.074902867
5	7	0.02	2	2	−3.041036036	−3.041096427
5	7	0.02	3	2	−3.012152597	−3.01211165
5	7	0.04	1	2	−3.074827609	−3.074844324
5	7	0.04	2	2	−3.041036036	−3.040768214
5	7	0.04	3	2	−3.012152597	−3.012079572

(*continued on next page*)

Table 3 (*continued*)

M	Re	Ec	Rd	CaseID	Cf_actual	Cf_pred
5	7	0.06	1	2	−3.074827609	−3.07481103
5	7	0.06	2	2	−3.041036036	−3.040412142
5	7	0.06	3	2	−3.012152597	−3.011825611
5	9	0.02	1	2	−3.445797482	−3.44581593
5	9	0.02	2	2	−3.409750082	−3.410477598
5	9	0.02	3	2	−3.377112274	−3.377161449
5	9	0.04	1	2	−3.445797482	−3.445827505
5	9	0.04	2	2	−3.409750082	−3.409909196
5	9	0.04	3	2	−3.377112274	−3.377193935
5	9	0.06	1	2	−3.445797482	−3.445770205
5	9	0.06	2	2	−3.409750082	−3.409649008
5	9	0.06	3	2	−3.377112274	−3.377207193

parameter of magnet M on the Nusselt number is depicted in Fig. 11**.** We find that as the parameter M increases. The Nusselt number, M, increases, which means that the heat transfer is enhanced. Further, Case-1 always has higher values than Case-2, which is positive in the rocket geometry applications that need to be thermally regulated efficiently. Fig. 12 demonstrates the influence of Reynolds number Re on the Nusselt number. It is observed that as the Reynolds number is higher, the Nusselt number is higher, which means enhanced convective heat transfer. Also, the values are a little bit higher in Case-1 than in Case-2, which is good, as far as rocket geometry is concerned, we need to have a good cooling performance.

4.2. Artificial neural networks through the Levenberg–Marquardt algorithm

By using the studies of Parida et al. [38,39], artificial neural networks with the Levenberg-Marquardt algorithm are fast and efficient, converging with improved gradient descent and Gauss-Newton algorithms. The method is very appropriate when dealing with the problem of nonlinear optimization, which returns a better accuracy. The architecture of a neural network in Fig. 13 contains an input layer with five neurons, two hidden layers (10 and 15 neurons) and an output layer (2 neurons). The structure displays weights, biases, and activation functions to map intricate input and output relationships, making it useful in predictive modelling and optimization exercises. Fig. 14 shows the results of the comparison between actual and predicted Nusselt numbers. The values calculated are near the ideal prediction line which indicates a high value of the model developed. This shows the accuracy of the method in estimating heat transfer in the geometry of a rocket.

The predicted values of skin friction are compared with the actual values in Fig. 15. The results show that the performance is very close to the speculative forecasting line, thus validating and proving the reliability of the model developed. It confirms its usefulness in analysing drag properties in rocket geometry studies. The training, validation and testing error vs. epochs is shown in Fig. 16 the convergence is gradual. The model is robust and reliable, with the mean squared error of 0.0029 at epoch 469. This means that it's used to predict and analyse rocket geometry. The changes in gradient, mu and validation checks with epochs are shown in Fig. 17. The gradient is starting to decrease slowly and the value of mu is kept very low and validation checks are also low, which means that the training process is efficient. This indicates the robustness and reliability of the neural network model. Fig. 18 shows the training, validation and testing and overall performance regression plots. The correlation coefficient is very close to 1, indicating that there is a perfect correlation between the predicted and the target. This validates the high predictive validity and reliability of the model developed. In Fig. 19, the error histogram shows the training, validation, and testing error distribution. The errors tend to be around zero, implying that the output obtained is close to the target output. This attests to the validity and extrapolation ability of the model developed. A comparison of ANN prediction and numerical results of skin friction is given in Table 3. The

Table 4
Table values for Nusselt number actual values vs ANN prediction.

M	Re	Ec	Rd	CaseID	Nu_actual	Nu_pred
1	5	0.02	1	1	4.939987	4.93999
1	5	0.02	2	1	7.834976	7.834974
1	5	0.02	3	1	10.79526	10.79972
1	5	0.04	1	1	4.298669	4.298664
1	5	0.04	2	1	6.876549	6.864041
1	5	0.04	3	1	9.53598	9.535975
1	5	0.06	1	1	3.65735	3.657351
1	5	0.06	2	1	5.918107	5.918101
1	5	0.06	3	1	8.276703	8.358264
1	7	0.02	1	1	6.006415	5.850012
1	7	0.02	2	1	9.489921	9.489907
1	7	0.02	3	1	13.04261	13.04259
1	7	0.04	1	1	5.311408	5.189388
1	7	0.04	2	1	8.449824	8.449813
1	7	0.04	3	1	11.67747	11.67746
1	7	0.06	1	1	4.616403	4.616395
1	7	0.06	2	1	7.409726	7.409712
1	7	0.06	3	1	10.31235	10.31233
1	9	0.02	1	1	6.896557	6.896541
1	9	0.02	2	1	10.87342	11.00335
1	9	0.02	3	1	14.92232	14.92229
1	9	0.04	1	1	6.14493	6.144911
1	9	0.04	2	1	9.746364	9.828575
1	9	0.04	3	1	13.44243	13.39218
1	9	0.06	1	1	5.393304	5.393288
1	9	0.06	2	1	8.619307	8.619286
1	9	0.06	3	1	11.96254	11.84015
3	5	0.02	1	1	2.85476	2.854762
3	5	0.02	2	1	4.623092	4.624491
3	5	0.02	3	1	6.489478	6.489478
3	5	0.04	1	1	2.514904	2.514902
3	5	0.04	2	1	4.117339	4.117338
3	5	0.04	3	1	5.828795	5.828797
3	5	0.06	1	1	2.175048	2.102652
3	5	0.06	2	1	3.611585	3.611584
3	5	0.06	3	1	5.168112	5.168111
3	7	0.02	1	1	3.542646	3.542637
3	7	0.02	2	1	5.708735	5.708726
3	7	0.02	3	1	7.979062	7.979057
3	7	0.04	1	1	3.172705	3.1727
3	7	0.04	2	1	5.158286	5.174928
3	7	0.04	3	1	7.261159	7.290746
3	7	0.06	1	1	2.802764	2.802753
3	7	0.06	2	1	4.607837	4.607832
3	7	0.06	3	1	6.543255	6.543251
3	9	0.02	1	1	4.126369	4.126357
3	9	0.02	2	1	6.62099	6.620979
3	9	0.02	3	1	9.220094	9.040951
3	9	0.04	1	1	3.726676	3.70619
3	9	0.04	2	1	6.025297	6.025279
3	9	0.04	3	1	8.442688	8.433032
3	9	0.06	1	1	3.326984	3.367397
3	9	0.06	2	1	5.429604	5.429587
3	9	0.06	3	1	7.665282	7.735684
5	5	0.02	1	1	2.050878	1.990314
5	5	0.02	2	1	3.338552	3.338554
5	5	0.02	3	1	4.71646	4.716467
5	5	0.04	1	1	1.820489	1.820491
5	5	0.04	2	1	2.995217	2.995218
5	5	0.04	3	1	4.267925	4.267919
5	5	0.06	1	1	1.5901	1.5901
5	5	0.06	2	1	2.651881	2.651883
5	5	0.06	3	1	3.81939	3.819397
5	7	0.02	1	1	2.507293	2.413171
5	7	0.02	2	1	4.083147	4.039334
5	7	0.02	3	1	5.76947	5.845481
5	7	0.04	1	1	2.253628	2.253623
5	7	0.04	2	1	3.705474	3.705468
5	7	0.04	3	1	5.27716	5.316684
5	7	0.06	1	1	1.999995	2.014682
5	7	0.06	2	1	3.327734	3.32773
5	7	0.06	3	1	4.78485	4.784848
5	9	0.02	1	1	2.910556	2.910547
5	9	0.02	2	1	4.734162	4.734151

(*continued on next page*)

Table 4 (*continued*)

M	Re	Ec	Rd	CaseID	Nu_actual	Nu_pred
5	9	0.02	3	1	6.679643	6.67963
5	9	0.04	1	1	2.634874	2.634863
5	9	0.04	2	1	4.323372	4.346131
5	9	0.04	3	1	6.144219	6.134598
5	9	0.06	1	1	2.359192	2.359181
5	9	0.06	2	1	3.912581	3.951662
5	9	0.06	3	1	5.608794	5.60878
1	5	0.02	1	2	4.914098	4.732471
1	5	0.02	2	2	7.791935	7.860733
1	5	0.02	3	2	10.73762	10.54332
1	5	0.04	1	2	4.262822	4.262835
1	5	0.04	2	2	6.819807	6.819808
1	5	0.04	3	2	9.461715	9.46171
1	5	0.06	1	2	3.611547	3.681551
1	5	0.06	2	2	5.847679	5.824892
1	5	0.06	3	2	8.185807	8.337523
1	7	0.02	1	2	5.974073	5.974072
1	7	0.02	2	2	9.435006	9.434997
1	7	0.02	3	2	12.9674	12.96738
1	7	0.04	1	2	5.265971	5.328252
1	7	0.04	2	2	8.376333	8.376324
1	7	0.04	3	2	11.57897	11.57896
1	7	0.06	1	2	4.557871	4.594377
1	7	0.06	2	2	7.317662	7.323122
1	7	0.06	3	2	10.19055	10.18723
1	9	0.02	1	2	6.858624	6.858612
1	9	0.02	2	2	10.80823	10.8082
1	9	0.02	3	2	14.8317	14.83167
1	9	0.04	1	2	6.091232	6.091218
1	9	0.04	2	2	9.658433	9.658412
1	9	0.04	3	2	13.32278	13.32275
1	9	0.06	1	2	5.323841	5.323832
1	9	0.06	2	2	8.50864	8.508618
1	9	0.06	3	2	11.81386	11.93918
3	5	0.02	1	2	2.832049	2.952016
3	5	0.02	2	2	4.586393	4.586394
3	5	0.02	3	2	6.441052	6.441052
3	5	0.04	1	2	2.487038	2.487046
3	5	0.04	2	2	4.073459	4.091461
3	5	0.04	3	2	5.771544	5.771545
3	5	0.06	1	2	2.142027	2.142037
3	5	0.06	2	2	3.560525	3.560528
3	5	0.06	3	2	5.102036	5.102037
3	7	0.02	1	2	3.510926	3.510922
3	7	0.02	2	2	5.658445	5.624403
3	7	0.02	3	2	7.912998	7.912988
3	7	0.04	1	2	3.134067	3.134067
3	7	0.04	2	2	5.098134	5.098129
3	7	0.04	3	2	7.182669	7.18266
3	7	0.06	1	2	2.757208	2.757211
3	7	0.06	2	2	4.53782	4.537813
3	7	0.06	3	2	6.45234	6.422356
3	9	0.02	1	2	4.087901	4.087891
3	9	0.02	2	2	6.560539	6.56052
3	9	0.02	3	2	9.140694	9.140674
3	9	0.04	1	2	3.679802	3.67979
3	9	0.04	2	2	5.952719	5.9527
3	9	0.04	3	2	8.347797	8.347774
3	9	0.06	1	2	3.271702	3.271688
3	9	0.06	2	2	5.344899	5.344884
3	9	0.06	3	2	7.5549	7.554879
5	5	0.02	1	2	2.034771	2.03478
5	5	0.02	2	2	3.311479	3.487054
5	5	0.02	3	2	4.679433	4.679432
5	5	0.04	1	2	1.800994	1.801001
5	5	0.04	2	2	2.963405	2.999107
5	5	0.04	3	2	4.22503	4.225034
5	5	0.06	1	2	1.567218	1.567229
5	5	0.06	2	2	2.61523	2.615234
5	5	0.06	3	2	3.770627	3.770628
5	7	0.02	1	2	2.481941	2.481938
5	7	0.02	2	2	4.04159	4.041585
5	7	0.02	3	2	5.713172	5.713173
5	7	0.04	1	2	2.223761	2.223762
5	7	0.04	2	2	3.657388	3.657384
5	7	0.04	3	2	5.212573	5.212561

Table 4 (*continued*)

M	Re	Ec	Rd	CaseID	Nu_actual	Nu_pred
5	7	0.06	1	2	1.96558	1.965579
5	7	0.06	2	2	3.273185	3.384341
5	7	0.06	3	2	4.711974	4.693177
5	9	0.02	1	2	2.877023	2.877012
5	9	0.02	2	2	4.680253	4.603023
5	9	0.02	3	2	6.607333	6.607314
5	9	0.04	1	2	2.595771	2.595756
5	9	0.04	2	2	4.261369	4.261352
5	9	0.04	3	2	6.0615	6.061486
5	9	0.06	1	2	2.314519	2.314509
5	9	0.06	2	2	3.842484	3.842471
5	9	0.06	3	2	5.515667	5.518901

results demonstrate a high level of agreement, indicating that both methods give similar results of high accuracy. Table 4 compares ANN predictions and numerical results of the Nusselt number. The values are near and show perfect correspondence, confirming the ANN model's authenticity.

5. Conclusion

The current paper has examined non-linear flow dynamics through a rocket geometry by considering the effects of magnetic parameter, radiation, viscous dissipation and porous effect and finding solutions to the modified governing equations based on Bvp4c solver in MATLAB tool. The mathematical modelling was related to ANN analysis, and the graphical and tabular comparisons were used to check the obtained results. Skin friction and Nusselt number were examined under different conditions, and the similarity between ANN results and numerical results proved the method's credibility. The results acquired are of great help in the optimization of thermal and flow performance in the rocket activity.

Key results of the current study

- Increasing the magnetic parameter significantly suppresses the velocity field due to the resistive Lorentz force, while improving the thermal boundary-layer thickness.
- The incorporation of Au-TiO_2-SiO_2 nanoparticles improves the thermophysical characteristics of the base fluid and improves thermal transport capability.
- Increases the radiation parameter values, raising the temperature profile, which shows its contribution to improving heat transport in fast rocket flows.
- Skin friction values are always greater in Case-2 than in Case-1, whereas Nusselt number values are slightly greater in Case-1.
- ANN predictions of the skin friction and the Nusselt number are very close to the numerical results, confirming the hybrid method's accuracy.
- The conjecture of convective heat transfer of rocket geometry is improved as the Reynolds numbers rise because it decreases thermal boundary layer thickness and skin friction.
- Viscous dissipation (Eckert number) also increases the temperature profile due to the additional heat generation in the flow.

Future research Directions

- Future studies may consider realistic rocket-engine cooling channel and convergent–divergent nozzle geometries to further enhance the engineering relevance of the model.
- The present investigation can be extended to compressible and turbulent flow regimes encountered in practical aerospace propulsion systems.

- The use of advanced machine-learning methods, like deep neural networks, ensemble learning, and physics-informed neural networks for enhanced predictive capability can be investigated.
- In some cases, multi-objective optimization methods can be used to simultaneously maximise the heat-transfer performance and minimize the flow resistance.
- Different ternary and quaternary combinations of nanoparticles can be studied to determine the best coolant combinations.
- Non-Newtonian base fluids, variable magnetic fields and nonlinear thermal radiation can be included to extend the range of the model presented in the current paper.

Limitations

- In the current study, only the laminar hybrid nanofluid flow between parallel plates is considered with the following physical assumptions.
- The numerical results are limited to the range of the governing parameters and boundary conditions selected.
- It is possible that the ANN model could overfit on small or highly correlated data sets.
- The training set used in the ANN is the most important factor in the prediction accuracy of the ANN and thus its size, quality, and representativeness are of critical importance.

CRediT authorship contribution statement

Gunisetty Ramasekhar: Writing – original draft, Software, Resources. **Maddina Dinesh Kumar:** Project administration, Methodology, Investigation. **A. Divya:** Visualization, Resources, Formal analysis. **Nehad Ali Shah:** Resources, Formal analysis, Conceptualization. **Se-Jin Yook:** Writing – review & editing, Validation, Supervision.

Declaration of competing interest

The authors declare that they have no known competing financial interests or personal relationships that could have appeared to influence the work reported in this paper.

Acknowledgement

This work was supported by the National Research Foundation of Korea (NRF) grant funded by the Korea government (MSIT) (RS-2024-00346834).

References

[1] Leishman JG. *Introduction to aerospace flight vehicles*. Embry-Riddle Aeronautical University; 2023.
[2] Daigle MJ, Smelyanskiy VN, Boschee J, Foygel M. Temperature stratification in a cryogenic fuel tank. J Thermophys Heat Transfer 2013;27(1):116–26.
[3] Farooq U, Waqas H, Imran M, Alghamdi M, Muhammad T. On melting heat transport and nanofluid in a nozzle of liquid rocket engine with entropy generation. J Mater Res Technol 2021;14:3059–69.
[4] Gasmi, H., Obalalu, A.M., Khan, U., Ishak, A., Gündoğdu, H., Abdullah, N., Elattar, S. and Galal, A.M., 2025. Analysis of advanced cooling strategies for rocket engines conveying ternary hybrid nanofluids with second slip conditions and melting heat transfer. *Case Studies in Thermal Engineering*, p.106312.
[5] Farooq, U., Han, Y., Liu, T., Sultan, H. and Alshamrani, A., 2026. Thermal Management of Rocket Nozzles Using MHD Copper-Ionic Liquid Nanofluid in Jeffery-Hamel Flow. Case Studies in Thermal Engineering, p.107752.
[6] Muhammad N, Ahmed N, Rani M, Mohsin BB. Application of deep learning to study aggregative and non-aggregative nanofluid flow within the nozzle of a liquid rocket engine. Int Commun Heat Mass Transfer 2024;155:107449.
[7] Ullah B, Rehman R, Wahab HA, Khan U, Emam W. Trihybrid nanofluid flow through nozzle of a rocket engine: Numerical solution and irreversibility analysis. Energy Explor Exploit 2025;43(1):302–18.
[8] Nazari S, Rezaei E, Moshizi A, S.,. Fluid Flow and Heat transfer of Nanofluids inside Helical Tubes at constant Wall Temperature. *ASME Journal of*. Heat Mass Transf 2025;147(5).
[9] Nabwey HA, Azizimehr B, Armaghani T, Ghasemiasl R, Alamdar NY, Rashad AM, et al. A COMPREHENSIVE REVIEW OF HEAT TRANSFER IN POROUS MEDIA: FOCUSING ON NANOFLUIDS, PHASE CHANGE MATERIALS, AND NANOENCAPSULATED PHASE CHANGE MATERIALS. Journal of Porous Media 2025;28(10).
[10] Yu G, Xu H. Application of Porous Media in Heat-Transfer and Mass-Transfer Enhancements. A Brief Review Transport Perspectives for Porous Medium Applications 2024.
[11] Hu X, Zhang B, Du X, Zhang H, Zhu T, Zhang S, et al. Recent advances and Future Perspectives on Heat and Mass transfer Mechanisms Enhanced by Preformed Porous Media in Vacuum Freeze-Drying of Agricultural and Food Products. Foods 2025;14(17):2966.
[12] Divya A, Reddy BA, P.. Entropy-optimized melting heat transport of Casson-Williamson hybrid nanofluid with blood-mediated nanoparticles over a rotating disk. Indian J Phys 2023;97(14):4337–52.
[13] Kumar A, Jayakumar JS, Babu JS. Modeling of thermal radiation in a participating media with conjugate heat transfer. Heat Transfer 2024;53(4):1949–74.
[14] Rashad AM, Kolsi L, Mansour MA, Salah T, Mir A, Armaghani T, et al. Effect of thermal radiation on unsteady magneto-hybrid nanofluid flow in a π-shaped wavy cavity saturated porous medium. Front Chem 2024;12:1441077.
[15] Majeed A, Saidani T, Ijaz N, Ibrahim AO, Gnaba H, Ali SS. Boost heat transfer efficiency through thermal radiation and electrical conductivity in nanofluids. ZAMM-Journal of Applied Mathematics and Mechanics/zeitschrift Für Angewandte Mathematik Und Mechanik 2024;104(12):e202400005.
[16] Qureshi, H., Latif, A., Athar, T., Raheem, A. and Muhammad, T., 2025. Artificial Neural Network Driven Investigation of thermal exchange through hybrid nanofluid of polymer/CNT across parallel sheets. *Case Studies in Thermal Engineering*, p.106903.
[17] Zubair M, Qureshi H, Hussain A, Khan WA, Muhammad T. Machine learning-based stochastic investigation of heat and momentum transfer in ternary-hybrid nanofluids with aggregation effects using artificial neural networks. J Therm Anal Calorim 2025;150(16):12567–85.
[18] Wang J, Zhai Y, Yao P, Ma M, Wang H. Established prediction models of thermal conductivity of hybrid nanofluids based on artificial neural network (ANN) models in waste heat system. Int Commun Heat Mass Transfer 2020;110.
[19] Parida C, Ratha SP, Mahanta G, Parija S, Shaw S. Multilayer neural network analysis of penta-hybrid nanofluid flow with entropy optimization: Application to rocket engine nozzle cooling. Eng Appl Artif Intel 2025;156:111106.
[20] Khan S, Mahmood Z, Popa IL, Liu S, Liu H, Ansari MA. Modelling of Ternary-Hybrid Nanofluid over Non-linear Radiative Inclined Cylinder under Soret-Dufour with Bioconvection and double Stratification Phenomena using Neural Network. Mater Today Commun 2025:114418.
[21] Mahmood Z, Rafique K, Abd-Elmonem A, Suoliman NA, Popa IL, Kumar A. Numerical and AI-based simulation of entropy generation in MHD Jeffery tetra nanofluid flow over an inclined cylinder for energy engineering applications. Eng Appl Comput Fluid Mech 2025;19(1):2580347.
[22] Wan A, Zhang H, Chen T, Al-Bukhaiti K, Wang W. A hybrid deep learning model for robust aeroengine remaining useful life prediction. SIViP 2025;19(7):550.
[23] Liu X, Yang S, Sun H, Wang Z, Guan X, Gu Y, et al. Review of deep learning-based aerodynamic shape surrogate models and optimisation for airfoils and blade profiles. Phys Fluids 2025;37(4).
[24] Haq F, Saleem M, Ghazwani HA, Ghazwani MH, Alnujaie A. Dynamics of radiated and stratified natural bioconvective flow of Cross hybrid nanomaterial with Darcy–Forchheimer and Lorentz force. ZAMM-Journal of Applied Mathematics and Mechanics/zeitschrift Für Angewandte Mathematik Und Mechanik 2025;105(9):e70224.
[25] Saleem M, Haq F, Ghazwani HA, Ghazwani MH, Alnujaie A. Mathematical modelling and theoretical investigation of entropy generation in bioconvective micropolar hybrid nanofluid flow with activation energy and Lorentz force. ZAMM-Journal of Applied Mathematics and Mechanics/zeitschrift Für Angewandte Mathematik Und Mechanik 2025;105(10):e70241.
[26] Kong D, Tian X, Li G, Liu C, Niu X, Isaev SA, et al. Numerical study of particle deposition and heat transfer characteristics in an S-shaped miniature cooling channel of a gas turbine blade. Powder Technol 2025:121612.
[27] Ye L, Zheng T, Wang X, Liang X, Liu C. Evaluating the heat transfer characteristics of mesh-fed slot cooling configuration: Influence of slot height and pin-fin arrangement. Appl Therm Eng 2025;271:126304.
[28] Rahman MU, Haq F, Ghazwani HA, Younis J, Ghazwani MH, Alnujaie A, et al. Physical aspects of entropy generation in magnetized mixed convection sutterby nanoliquid flow with chemical reaction. Int J Energy Res 2025;2025(1):9310834.
[29] Khouqeer GA, Haq F, Rahman MU, Sallah M. An investigation of thermo-bioconvective ternary hybrid nanofluid flow over rotating disk subject to activation energy. J Therm Anal Calorim 2025;150(18):14673–85.
[30] Ahmad S, Santos EDD, Ali K, Junjua MUD, Mahmood Z, Rashid FL, et al. The role of machine learning in analyzing magnetic field localization and vortex generation in tetra-hybrid nanofluid: a numerical study. Mod Phys Lett B 2025;39(25):2550115.
[31] Mahmood Z, Rafique K, Ansari MA, Ahmed N, Khan U, Kumar A, et al. Deep learning investigation of water-based tetra hybrid nanofluid across a shrinking cylinder for variable electrical conductivity with thermal radiation. J Radiat Res Appl Sci 2025;18(1):101213.
[32] Sakkaravarthi K, Reddy PBA, Sakthi I. Entropy optimization in Casson tetra-hybrid nanofluid flow over a rotating disk with nonlinear thermal radiation: a Levenberg–Marquardt neural network approach. J Comput Des Eng 2024;11(5):333–54.
[33] Singh SP, Kumar M, Yaseen M, Rawat SK. Ternary hybrid nanofluid (TiO2− SiO2−MoS2/kerosene oil) flow over a rotating disk with quadratic thermal radiation and Cattaneo-Christov model. J Cent South Univ 2023;30(4):1262–78.
[34] Mahanta G, Parida C, Meher D, Shaw S. Entropy and thermal optimization on electromagnetic Darcy–Forchheimer trihybrid nanofluid flow with regression and

sensitivity analysis: G. Mahanta et al. J Therm Anal Calorim 2025;150(18): 14583–602.
[35] Pattnaik PK, Shamshuddin MD, Panda S, Mishra SR, Eid MR. Modified Adomian decomposition mechanism for hybrid nanofluid flow through rocket engine nozzle based CoFe2O4 and Ag nanoparticles. Chaos, Solitons Fractals 2025;197:116521.
[36] Ullah B, Rehman R, Wahab HA, Khan U, Abd-Elmonem A, Suoliman NA. Irreversibility analysis for nanofluid flow in a rocket engine with MHD effects. ZAMM-Journal of Applied Mathematics and Mechanics/zeitschrift Für Angewandte Mathematik Und Mechanik 2025;105(3):e202400281.
[37] Acharya N, Das K, Kundu PK. On the heat transport mechanism and entropy generation in a nozzle of liquid rocket engine using ferrofluid: a computational framework. J Comput Des Eng 2019;6(4):739–50.
[38] Parida C, Lekgari MV, Mahanta G, Shaw S. Multi-layer neural network on 3D transition metal hydrides-based ternary nanofluid flow with entropy: Application to spinning disk reactor. Therm Sci Eng Prog 2025;62:103641.
[39] Parida C, Mahanta G, Shaw S. Nonlinear fractional hemodynamic modeling of trihybrid Jeffrey nanofluid in stenosed arteries with artificial neural networks and K-fold cross-validation. Phys Fluids 2025;37(11).

fx1**Nehad Ali Shah** Currently, I am an Assistant Professor in the Department of Mechanical Engineering, Sejong University, Seoul, South Korea. I completed one year Post-Doctoral from Department of Mechanical Engineering, Sejong University, Seoul, South Korea. I received my PhD degree from Abdus Salam School of Mathematical Sciences, Government College University, Lahore, Pakistan. I was awarded a Pre-PhD quality research award in 2018 from Abdus Salam School of Mathematical Sciences, Government College University, Lahore, Pakistan and Research Excellence Professor Award in 2024 from Sejong University, Seoul, South Korea. Till now my more than 600 research papers have been published in prestigious journals in which many of them are listed highly cited. Also, I am a co-author of on book published online with Chapman and Hall/CRC. A leading author of the one book chapter. I included in the list of the Top 2% Scientist Data given by Stanford University, USA (2020-2021), (2021-2022), (2022-2023), (2023-2024) and (2024-2025) respectively, with serial numbers (S# 160229), (S# 84069), (S# 39120), (S# 20509) and (S# 14680). On ScholarGPS, I am listed “Highly Ranked Scholar – Prior Five Years 2024” in the disciplines of “All filed of Scholarly Endeavor (#1857), Engineering and Computer Science (#816), Mechanical Engineering (#87)”. I am an Editorial board member of 10 journals and reviewing for more than 60 journals.